Engineering of octahedral rotations and electronic structure in ultrathin SrIrO_{3} films

W. Guo, D. X. Ji, Z. B. Gu, J. Zhou, Y. F. Nie, and X. Q. Pan

Phys. Rev. B **101**, 085101 — Published 3 February 2020

DOI: 10.1103/PhysRevB.101.085101

Engineering of octahedral rotations and electronic structure in ultrathin $SrIrO_3$ films

W. Guo,[1] D.X. Ji,[1] Z.B. Gu,[1] J. Zhou,[1, *] Y.F. Nie,[1, †] and X.Q. Pan[1, 2]

[1]*National Laboratory of Solid State Microstructures, College of Engineering and Applied Sciences,*
and Collaborative Innovation Center of Advanced Microstructures, Nanjing University, Nanjing 210093, China
[2]*Department of Chemical Engineering and Materials Science and Department of Physics and Astronomy,*
University of California, Irvine, 916 Engineering Tower, Irvine, California 92697, USA

Layered perovskite iridate Sr_2IrO_4 shares many similarities with high T_c cuprates and is expected to host novel superconductivity but has never been realized experimentally. Despite the similarities, the prominent IrO_6 octahedral rotations and sizable net canted antiferromagnetic moments lying in each IrO_2 plane in Sr_2IrO_4 are strikingly different from high T_c cuprates where the octahedral rotations and net canted moment are much smaller or negligible. Here, using reactive molecular beam epitaxy, we demonstrate that the octahedral rotations around the in-plane and out-of-plane axises in epitaxial iridate films can be suppressed step-by-step via interfacial clamping imposed by cubic substrates as the films approach the two-dimensional limit. *In situ* angle-resolved photoemission spectroscopy (ARPES) and first-principles calculations show a gapped antiferromagnetic ground state with dispersive low-lying bands in 1- and 2-unit-cell-thick $SrIrO_3$ films, providing ideal single- and bi-layer analogies of high T_c cuprates.

PACS numbers:
Keywords:

Ruddlesden-Popper (RP) type layered perovskite iridate, Sr_2IrO_4, has drawn great attention since they have been predicted to host novel high-T_c superconductivity with the Cooper pairs formed by $5d$ electrons [1, 2]. In particular, Sr_2IrO_4 shares many similarities with high-T_c cuprates, including the layered crystalline structure [3], (pseudo) spin 1/2 states [4–6], antiferromagnetic Mott insulating ground state [7], Fermi arcs [8, 9], d-wave-like and V shape energy gaps [10–12]. Nonetheless, direct evidences of superconductivity such as zero resistivity and Meissner effect are still lacking up to date. Despite so many similarities have been observed between iridates and cuprates, the exact lattice structure and antiferromagnetic ordering in Sr_2IrO_4 are actually strikingly different from cuprates. Superconducting cuprates exhibit zero or tiny octahedral rotations and the antiferromagnetic ordering in their undoped parent compounds shows zero or negligible net canted moments [13, 14]. Experimental studies imply that the lattice distortion from a perfect square CuO_2 plane may suppress the superconductivity in cuprates [15]. In Sr_2IrO_4, however, the cooperative interplay of strong spin-orbit coupling (SOC), electron correlations and large octahedral rotations (about the c axis by $\sim 12^\circ$) results in a canted antiferromagnetic ground state with sizable net magnetic moments ($0.14\ \mu_B/Ir^{4+}$) lying in IrO_2 planes (see Fig. 1a) [6, 16, 17]. This breaks the time reversal symmetry and may hinder the expected superconductivity in iridates when the net canted moment is above a certain critical value. Note that the sister compound Ba_2IrO_4 exhibits no IrO_6 octahedral rotations, however, the effective charge carrier doping in Ba_2IrO_4 is difficult and more metallic states require the application of high pressure [18, 19], which may cause octahedral rotations and also prevent direct measurements of its electronic structure by ARPES and scanning tunneling microscope(STM). Therefore, suppressing the octahedral rotations and canted moments in Sr_2IrO_4 may shed light on the exploration of novel high T_c superconductivity in iridates.

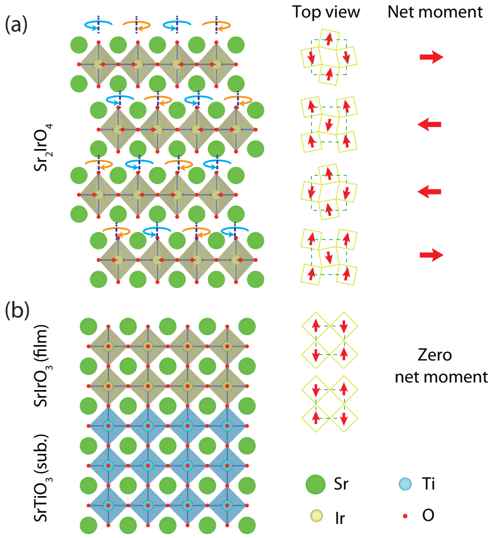

FIG. 1: (a) Schematics of the octahedral rotations, canted antiferromagnetic ordering and net magnetic moments in Sr_2IrO_4. (b) Suppression of the octahedral rotations and canted moments via interfacial clamping imposed by a cubic substrate.

In addition to the layered perovskite Sr_2IrO_4, its three dimensional counterpart $SrIrO_3$ has been recently employed as the key building blocks to construct quasi-two-dimensional IrO_6 octahedron network in forms of superlattices [20, 21] and ultrathin films [22, 23]. Bulk crystal

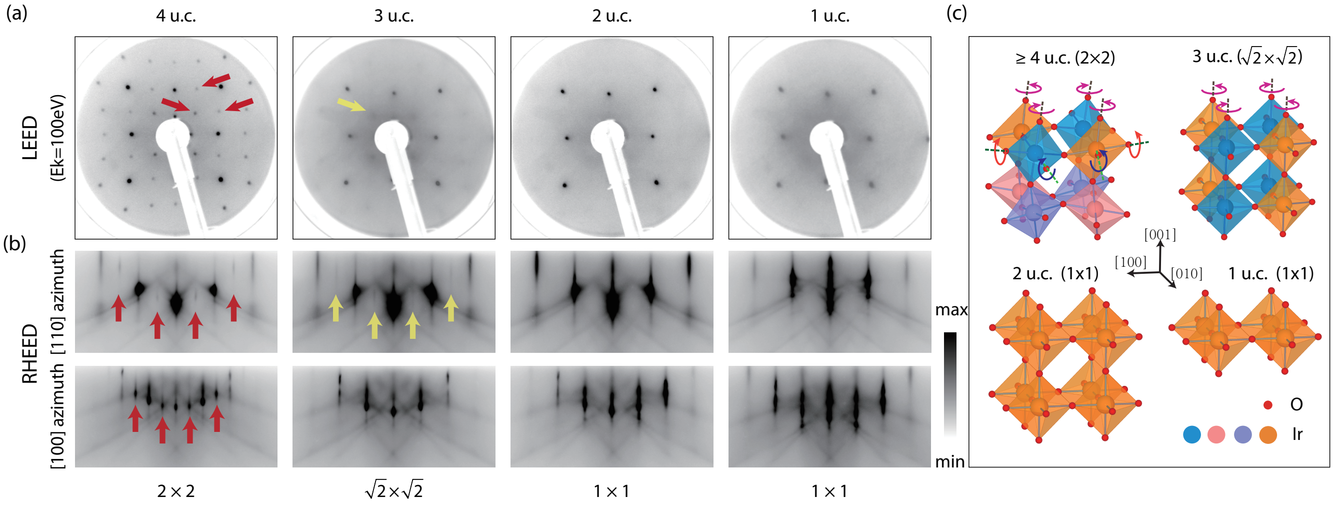

FIG. 2: The evolution of the superstructure diffractions in (a) LEED patterns taken at 150K and (b) RHEED patterns taken at 200 °C on $SrIrO_3$ films indicates the suppression of the octahedral rotations around in-plane axises in 3 u.c. film and the full suppression of all rotations in 2 u.c. and 1 u.c films. Red and yellow arrows point to the superstructure diffractions with respect to the the undistorted cubic unit cell. (c) The schematics of the octahedral rotations in ultrathin epitaxial $SrIrO_3$ films.

and thick films of $SrIrO_3$ are paramagnetic semi-metal with the Fermi surface consisted of electron and hole-like pockets [24–26]. In $[SrIrO_3]_n/[SrTiO_3]_1$ superlattices, a paramagnetic semi-metal to canted antiferromagnetic insulator transition takes place as the $SrIrO_3$ layers become thinner than $n = 3$ [20, 21, 27]. Recent work by Schütz et al. reports the observation of a dimensionality-driven gap opening between 4 and 3 unit cell (u.c.) $SrIrO_3$ films, which is accompanied with the partial suppression of the octahedral rotations [23]. Nonetheless, whether the octahedral rotations and the weak ferromagnetism can be fully suppressed in Sr-based iridates remains an open question.

In this letter, using reactive molecular beam epitaxy, we demonstrate that the octahedral rotations can be fully suppressed in ultrathin epitaxial $SrIrO_3$ films via interfacial clamping imposed by cubic substrates(Fig. 1b). *In situ* ARPES and first-principles calculations show gapped antiferromagnetic ground state with dispersive low-lying bands in 2 u.c. and 1 u.c. $SrIrO_3$ films, providing ideal bi-layer and single-layer analogies of high T_c cuprates.

A series of $SrIrO_3$ films of various thicknesses were grown on (001) $SrTiO_3$ substrates by reactive molecular beam epitaxy (MBE) with an oxidant (distilled O_3) background pressure of 5×10^{-6} Torr and at a substrate temperature of 850 °C. Following the growth, $SrIrO_3$ films were transferred through ultra-high vacuum ($< 1 \times 10^{-10}$ Torr) into a high-resolution ARPES system with a VG Scienta R8000 electron analyzer and a VUV5000 helium plasma discharge lamp. ARPES measurements were performed using He Iα ($h\nu = 21.2$ eV) photons with an energy resolution ΔE of 11 meV. Crystalline quality of $SrIrO_3$ films were measured by a lab-based high resolution four circle x-ray diffractometer and the surface lattice structures were measured by *in situ* reflection high-energy electron diffraction (RHEED) and low energy electron diffraction (LEED). First-principles density functional theory (DFT) calculations of bulk and slabs of $SrIrO_3$ were performed within the GGA-PBE approximation using the VASP package. More details regarding the film growth, characterizations and theoretical calculations can be found in the Supplemental Material [28] .

The octahedral rotations in $SrIrO_3$ films strongly depend on the film thickness, which can be probed by diffraction techniques. As shown in Fig. 2, LEED patterns taken on a 4 u.c. and thicker $SrIrO_3$ film exhibits a 2×2 surface reconstruction with respect to the undistorted cubic unit cell, indicating the coexistence of rotations along the in-plane and out-of-plane axies as reported in bulk samples and thick $SrIrO_3$ films [25, 39]. Consistently, the RHEED patterns taken along the [110] and [100] azimuth directions show clear half order diffractions (red arrows). As the film thickness decreases to 3 u.c., LEED pattern mainly show $\sqrt{2} \times \sqrt{2}$ reconstruction spots, and the half-order diffractions only remain in the RHEED patterns taken along the [110] azimuth direction. These indicate that IrO_6 octahedral rotations around the in-plane axis disappear but the octahedral rotations around the out-of-plane axis still exist, which is consistent with the recent report on ultrathin $SrIrO_3$ films by Schütz et al. [23] and resembles the rotation pattern in Sr_2IrO_4 [40]. Interestingly, further decreasing the

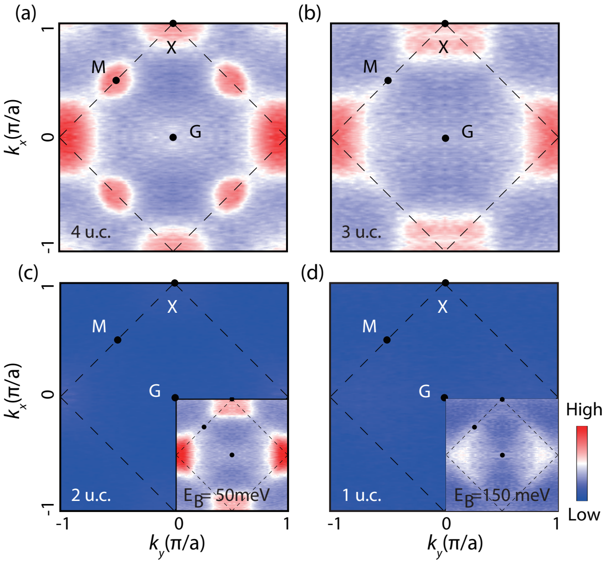

FIG. 3: (a) Fermi surface mapping of a 4 u.c. $SrIrO_3$ film, showing the coexistence of electron and hole-like pockets around X and M points, respectively. (b) The electron pockets disappear in the 3 u.c. film. Both electron and hole-like pockets disappear in (c) 2 u.c. and (d) 1 u.c. $SrIrO_3$ films. Inset figures in (c) and (d) show iso-energy maps taken at higher binding energies. All ARPES measurements were performed at 150 K.

film thickness to 2 u.c. and 1 u.c., LEED and RHEED patterns show no superstructure diffractions, indicating the full suppression of both in-plane and out-of-plane octahedral rotations in these ultrathin films. Note that LEED and RHEED techniques are extremely surface sensitive and has been employed to characterize tiny surface reconstructions in the field of surface science [41, 42]. All of our films are terminated with SrO layer in order to preserve the complete IrO_6 octahedral symmetry by specifically deposit an extra SrO layer on TiO_2 terminated $SrTiO_3$ substrate before the MBE growth of $SrIrO_3$ films (Supplemental Material Fig. S2 [28]). Due to the dangling bonds on the IrO_2 surface, the IrO_2 terminated films form surface reconstructions and exhibit $\sqrt{2} \times \sqrt{2}$ reconstruction spots in both RHEED and LEED patterns (Supplemental Material Fig. S4 [28]), which may explain why 2 u.c. and 1 u.c. $SrIrO_3$ films grown by pulsed laser deposition (PLD) show reconstruction diffractions [23]. We should also point out that the low temperature phases of $SrTiO_3$ are not cubic [43], but the octahedral rotations are small and negligible as that in cuprates. Other cubic substrates can be also used to engineer the octahedral rotations of iridates in future experiments.

The different critical thickness for the relaxation of octahedral rotations around the in-plane and out-of-plane axises are interesting and mostly likely due to the different bonding conditions. Moreover, the critical thickness for octahedral rotation relaxation is strikingly shorter than strain relaxation. The 30 u.c. SrIrO3 film grown on $SrTiO_3$ substrate is still fully strained without any relaxation (Supplemental Material Fig. S1(c) [28]), while the octahedral rotations start to relax in 3 u.c. and the whole rotation pattern is recovered in 4 u.c. $SrIrO_3$ films. Our observations indicate that the engineering of octahedral rotations can only be effectively performed in ultrathin films. The suppression of octahedral rotations by interfacial clamping is also supported by our theoretical calculations (Supplemental Material Fig. S8 [28]). The energy gain with octahedral rotations is significantly lowered due to the substrate clamping and the zero-rotation configuration becomes more stable in the structure with thicker $SrTiO_3$ substrate layer. Only thick enough $SrTiO_3$ layer can win the competition and suppress the octahedral rations in $SrIrO_3$ films. This also explains the existance of octahedral rotations and canted antiferromagnetism in previous works on $[(SrIrO_3)_n/(SrTiO_3)_m]$ superlattices with thin $SrTiO_3$ layers [21, 27].

The electronic structures of $SrIrO_3$ films also show strong dependence on the film thickness and octahedral distortions (Fig. 3). For thicker ($\geq$ 4 u.c.) films, Fermi surface maps show the coexistence of hole-like pockets around X points ($(\pm\pi, 0)$ and $(0, \pm\pi)$) and electron pockets around M points $(\pm\pi/2, \pm\pi/2)$, consistent with the previously report in thick $SrIrO_3$ films [25, 26]. As shown in Fig. 4, the E vs k spectra taken along the high symmetric momenta are consistent with the Fermi surface maps, showing the disappearing of electron bands in 3 u.c. and thinner films. These results indicate the gap opening between 4 u.c. and 3 u.c. $SrIrO_3$ films, which is consistent with the recent report by Schütz et al. [23]. The reason why the Fermi surface of 3 u.c. film shows hole-like bands is most likely due to the slightly imperfect stoichiometry of this film. It is known that IrO_x is volatile and slight Ir deficiency could effectively dope holes in the films [25, 44]. Nonetheless, these results indicate the gap opening as the film thickness approaches the two-dimensional limit.

By fitting the momentum distribution curves (MDCs) and energy distribution curves (EDCs) (Supplemental Material Fig. S5 [28]), we extract the band dispersion of the hole-like bands along the (0,0)-(0,π)-(0,2π) high symmetric momenta (Fig. 4b). We simply fit the hole-like bands with a parabolic function to extract the “effective mass” to uncover the evolution of band dispersion (Fig. 4c). As the film thickness decreases, the fitted “effective mass” gradually increases from 1.0 electron rest mass (m_e) for 6 u.c. film to 1.2 m_e for 3 u.c. film. The enhancement of the effective mass is due to the decrease of the number of nearest neighboring hopping sites in thinner films, which narrows the band width W and increases the effective correlations U/W [24].

In addition to the dimensionality driven effective mass enhancement, the octahedral rotations also have strong

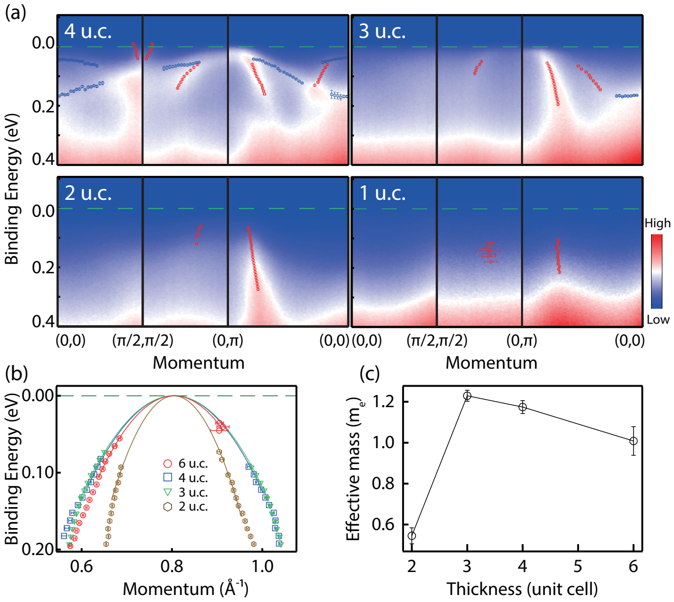

FIG. 4: (a) E *vs* k dispersions along the high-symmetry momenta of $SrIrO_3$ films of various thicknesses.The blue and red symbols are the extracted peaks by fitting the energy dispersion curves (MDCs) and momentum distribution curves (EDCs) using Lorentzian and Gaussian functions, respectively. (b) Extracted hole-like bands along (0,0)-(0,π)-(0,2π) momenta with the valence band tops aligned at the Fermi level. (c) Effective masses extracted by parabolic fits to the hole-like bands shown in (b).

impact on the band dispersion. The suppression of the rotations around the out-of-plane axis in 2 u.c. and 1 u.c. films straightens the Ir-O-Ir bonding, which significantly enhances the in-plane hopping and reduces the "effective mass" by a factor of 2. We should point out that the electronic structure of bulk $SrIrO_3$ is three dimensional in nature while our lab-based ARPES measurements with fixed-energy photons only probe the states of a very narrow kz range. However, the calculated hole-like bands around (0, π) of bulk $SrIrO_3$ only show minor k_z dependence and the above discussion of the effective mass should still valid in a qualitative level. Note that 2 u.c. (1 u.c.) $SrIrO_3$ film is consist of two (one) layers of corner-shared IrO_6 planes and can be essentially viewed as bilayer (monolayer) systems. Compared to the bilayer $Sr_3Ir_2O_7$ [29] and monolayer Sr_2IrO_4 [31], the low lying bands of our 2 u.c. and 1 u.c. $SrIrO_3$ films are much more dispersive (Supplemental Material Fig. S6 [28]), revealing the pivotal role of the octahedral rotations on the electronic band structure.

We also performed first-principles density functional theory (DFT) calculations to explore the magnetic ground states in these ultrathin $SrIrO_3$ films. Direct experimental measurements on the antiferromagnetic ordering in such ultrathin iridate films are extremely challenging and formidable. As shown in Table I, the DFT+SOC+U calculations show that the insulating antiferromagnetic state is much more stable than the nonmagnetic or ferromagnetic states for both 2 u.c. and 1 u.c. $SrIrO_3$. Consistently, antiferromagnetic ground states were reported in low dimensional iridates, such as single layer, bilayer, ultrathin films and superlattices of iridates [8, 17, 23, 45, 46]. Interestingly, the antiferromagnetic order with spins lying in-plane along the Ir-O-Ir bonding direction are energetically most stable in both 2 u.c. and 1 u.c. $SrIrO_3$ slabs. In bulk iridates, the spins in single-layer Sr_2IrO_4 lie in-plane [17] while the spins in bi-layer $Sr_3Ir_2O_7$ lie along the out-of-plane direction [47]. In fact, the driving force for the spin configurations in layered iridates is highly nontrivial. For example, whether intra- or inter-plane interactions play more important role, in stabling the basal antiferromagnetic ordering in Sr_2IrO_4 is still under debate [48–50]. The underlying mechanism why the spin configuration of a 2 u.c. $SrIrO_3$ slab is different from bi-layer $Sr_3Ir_2O_7$ is out of the scope of this experimental work but it is an interesting problem to be explored in the future.

TABLE I: Calculated total energy as a function of magnetic ordering and film thickness.

Energy (meV) per Ir ion	**1 u.c.**	**2 u.c.**
AFM (spin lies along in plane Ir-O-Ir direction)	0	0
AFM (spin lies along in plane and 45° from Ir-O-Ir direction)	0.19	0.22
AFM (spin lies along out-of-plane direction)	0.79	0.74
Non magnetic	43.43	31.33
Ferromagnetic (spin lies along in plane and 45° from Ir-O-Ir direction)	41.76 (relaxed to near zero spin moment)	31.33 (relaxed to zero spin moment)

In summary, by a combination of MBE, LEED, RHEED, ARPES and DFT calculations, we demonstrate that the octahedral rotations, electronic structure and magnetic ground state in ultrathin epitaxial $SrIrO_3$ films can be engineered via interfacial clamping imposed by cubic substrates. When approaching the two dimensional limit, the octahedral rotations around the in-plane and out-of-plane axises are suppressed step-by-step in ultrathin $SrIrO_3$ films grown on $SrTiO_3$ substrate. The low dimensionality and straight Ir-O-Ir bonding in 2 u.c. and 1 u.c. $SrIrO_3$ films result in an antiferromagneitc ground state with dispersive low-lying hole-like bands, providing ideal bilayer and single-layer systems for exploring novel superconductivity in 5d iridates upon charge carrier doping.

This work is supported by National Basic Research Program of China (Grant Nos. 2015CB654901), the National Key R&D Program of China (2016YFA0201104), the National Natural Science Foundation of China (No. 11774153, 11574135, 51672125), and the Fundamental Research Funds for the Central Universities (No. 0213-14380058). The use of the computational resources in the High Performance Computing Center of Nanjing University for this work is also acknowledged. Work at UCI was supported by NSF grant No. DMR-1807817.

---

[*] Electronic address: `zhoujian@nju.edu.cn`
[†] Electronic address: `ynie@nju.edu.cn`

[1] F. Wang and T. Senthil, Phys. Rev. Lett. **106**, 136402 (2011).
[2] Y. Yang, W. S. Wang, J. G. Liu, H. Chen, J. H. Dai, and Q. H. Wang, Phys. Rev. B **89**, 094518 (2014).
[3] J. J. Randall, L. Katz, and R. Ward, J. Am. Chem. Soc. **79**, 266 (1957).
[4] B. Kim, H. Jin, S. Moon, J. Y. Kim, B. G. Park, C. Leem, J. Yu, T. Noh, C. Kim, S. J. Oh, et al., Phys. Rev. Lett. **101**, 076402 (2008).
[5] H. Watanabe, T. Shirakawa, and S. Yunoki, Phys. Rev. Lett. **110**, 027002 (2013).
[6] B. Kim, H. Ohsumi, T. Komesu, S. Sakai, T. Morita, H. Takagi, and T. h. Arima, Science **323**, 1329 (2009).
[7] J. Kim, D. Casa, M. Upton, T. Gog, Y. J. Kim, J. Mitchell, M. Van Veenendaal, M. Daghofer, J. van Den Brink, G. Khaliullin, et al., Phys. Rev. Lett. **108**, 177003 (2012).
[8] Y. Kim, O. Krupin, J. Denlinger, A. Bostwick, E. Rotenberg, Q. Zhao, J. Mitchell, J. Allen, and B. Kim, Science **345**, 187 (2014).
[9] A. De La Torre, S. M. Walker, F. Y. Bruno, S. Riccó, Z. Wang, I. G. Lezama, G. Scheerer, G. Giriat, D. Jaccard, C. Berthod, et al., Phys. Rev. Lett. **115**, 176402 (2015).
[10] Y. Kim, N. Sung, J. Denlinger, and B. Kim, Nature Phys. **12**, 37 (2016).
[11] Y. Yan, M. Ren, H. Xu, B. Xie, R. Tao, H. Choi, N. Lee, Y. Choi, T. Zhang, and D. Feng, Phys. Rev. X **5**, 041018 (2015).
[12] I. Battisti, K. M. Bastiaans, V. Fedoseev, A. De La Torre, N. Iliopoulos, A. Tamai, E. C. Hunter, R. S. Perry, J. Zaanen, F. Baumberger, et al., Nature Phys. **13**, 21 (2017).
[13] T. Thio, T. Thurston, N. Preyer, P. Picone, M. Kastner, H. Jenssen, D. Gabbe, C. Chen, R. Birgeneau, and A. Aharony, Phys. Rev. B **38**, 905 (1988).
[14] G. De Luca, G. Ghiringhelli, M. M. Sala, S. Di Matteo, M. Haverkort, H. Berger, V. Bisogni, J. Cezar, N. Brookes, and M. Salluzzo, Phys. Rev. B **82**, 214504 (2010).
[15] T. Schütz, R. Smith, A. Fondado, C. Maley, T. Beacom, P. Tinklenberg, J. Gross, C. Saylor, S. Oseroff, Z. Fisk, et al., J. Appl. Phys. **75**, 6723 (1994).
[16] G. Cao, J. Bolivar, S. McCall, J. E. Crow, and R. P. Guertin, Phys. Rev. B **57**, R11039 (1998).
[17] F. Ye, S. Chi, B. C. Chakoumakos, J. A. Fernandez-Baca, T. Qi, and G. Cao, Phys. Rev. B **87**, 140406 (2013).
[18] H. Okabe, M. Isobe, E. Takayama-Muromachi, N. Takeshita, and J. Akimitsu, Phys. Rev. B **88**, 075137 (2013).
[19] H. Okabe, M. Isobe, E. Takayama-Muromachi, A. Koda, S. Takeshita, M. Hiraishi, M. Miyazaki, R. Kadono, Y. Miyake, and J. Akimitsu, Phys. Rev. B **83**, 155118 (2011).
[20] D. Meyers, Y. Cao, G. Fabbris, N. J. Robinson, L. Hao, C. Frederick, N. Traynor, J. Yang, J. Lin, M. Upton, et al., Sci. Rep. **9**, 4263 (2019).
[21] J. Matsuno, K. Ihara, S. Yamamura, H. Wadati, K. Ishii, V. V. Shankar, H.-Y. Kee, and H. Takagi, Phys. Rev. Lett. **114**, 247209 (2015).
[22] D. Groenendijk, C. Autieri, J. Girovsky, M. C. Martinez-Velarte, N. Manca, G. Mattoni, A. Monteiro, N. Gauquelin, J. Verbeeck, A. Otte, et al., Phys. Rev. Lett. **119**, 256403 (2017).
[23] P. Schütz, D. Di Sante, L. Dudy, J. Gabel, M. Stübinger, M. Kamp, Y. Huang, M. Capone, M. A. Husanu, V. Strocov, et al., Phys. Rev. Lett. **119**, 256404 (2017).
[24] S. Moon, H. Jin, K. W. Kim, W. Choi, Y. Lee, J. Yu, G. Cao, A. Sumi, H. Funakubo, C. Bernhard, et al., Phys. Rev. Lett. **101**, 226402 (2008).
[25] Y. Nie, P. King, C. Kim, M. Uchida, H. Wei, B. Faeth, J. Ruf, J. Ruff, L. Xie, X. Pan, et al., Phys. Rev. Lett. **114**, 016401 (2015).
[26] Z. Liu, M. Li, Q. Li, J. Liu, W. Li, H. Yang, Q. Yao, C. Fan, X. Wan, Z. Wang, et al., Sci. Rep. **6**, 30309 (2016).
[27] L. Hao, D. Meyers, C. Frederick, G. Fabbris, J. Yang, N. Traynor, L. Horak, D. Kriegner, Y. Choi, J.-W. Kim, et al., Phys. Rev. Lett. **119**, 027204 (2017).
[28] *See Supplemental Material at [URL will be inserted by publisher] for detailed information of the sample growth, characterizations, and theoretical calculations, which includes Refs. [4,23,29-37].*
[29] M. Uchida, Y. Nie, P. King, C. Kim, C. Fennie, D. Schlom, and K. Shen, Phys. Rev. B **90**, 075142 (2014).
[30] P. King, T. Takayama, A. Tamai, E. Rozbicki, S. M. Walker, M. Shi, L. Patthey, R. Moore, D. Lu, K. Shen, et al., Phys. Rev. B **87**, 241106 (2013).
[31] Q. Wang, Y. Cao, J. Waugh, S. Park, T. Qi, O. Korneta, G. Cao, and D. Dessau, Phys. Rev. B **87**, 245109 (2013).
[32] B. M. Wojek, M. Berntsen, S. Boseggia, A. Boothroyd, D. Prabhakaran, D. McMorrow, H. Rønnow, J. Chang, and O. Tjernberg, J. Phys. Condens. Matter **24**, 415602 (2012).
[33] G. Affeldt, T. Hogan, J. D. Denlinger, A. Vishwanath, S. D. Wilson, and A. Lanzara, Phys. Rev. B **97**, 125111 (2018).
[34] G. Kresse and J. Hafner, Phys. Rev. B **48**, 13115 (1993).
[35] G. Kresse and J. Furthmüller, Comp. Mater. Sci. **6**, 15 (1996).
[36] P. E. Blöchl, Phys. Rev. B **50**, 17953 (1994).
[37] G. Kresse and D. Joubert, Phys. Rev. B **59**, 1758 (1999).
[38] J. P. Perdew, K. Burke, and M. Ernzerhof, Phys. Rev. Lett. **77**, 3865 (1996).
[39] F. X. Wu, J. Zhou, L. Zhang, Y. Chen, S.-T. Zhang, Z. B. Gu, S.-H. Yao, and Y. F. Chen, J. Phys. Condens. Matter **25**, 125604 (2013).
[40] Q. Li, G. Cao, S. Okamoto, J. Yi, W. Lin, B. C. Sales, J. Yan, R. Arita, J. Kuneš, A. V. Kozhevnikov, et al., Sci. Rep. **3** (2013).

[41] K. Oura, V. Lifshifts, A. Saranin, A. V. Zotov, and M. Katayama, *Surface Science* (Springer-Verlag, Berlin Heidelberg New York, 2003).

[42] A. Ichimiya and P. I. Cohen, *Reflection high-energy electron diffraction* (Cambridge University Press, 2004).

[43] H. Unoki and T. Sakudo, J. Phys. Soc. Jpn. **23**, 546 (1967).

[44] E. H. P. Cordfunke and G. Meyer, Recl. Trav. Chim. Pays-Bas **81**, 495 (1962).

[45] J. W. Kim, Y. Choi, J. Kim, J. F. Mitchell, G. Jackeli, M. Daghofer, J. van den Brink, G. Khaliullin, and B. J. Kim, Phys. Rev. Lett. **109**, 037204 (2012).

[46] S. Fujiyama, K. Ohashi, H. Ohsumi, K. Sugimoto, T. Takayama, T. Komesu, M. Takata, T. Arima, and H. Takagi, Phys. Rev. B **86**, 174414 (2012).

[47] S. Boseggia, R. Springell, H. C. Walker, A. T. Boothroyd, D. Prabhakaran, S. P. Collins, and D. F. McMorrow, J. Phys.: Condens. Matter. **24**, 312202 (2012).

[48] S. Boseggia, R. Springell, H. Walker, H. M. Rønnow, C. Rüegg, H. Okabe, M. Isobe, R. Perry, S. Collins, and D. McMorrow, Phys. Rev. Lett. **110**, 117207 (2013).

[49] V. M. Katukuri, V. Yushankhai, L. Siurakshina, J. V. D. Brink, L. Hozoi, and I. Rousochatzakis, Phys. Rev. X **4**, 021051 (2014).

[50] Y. Hou, H. Xiang, and X. Gong, New J. Phys. **18**, 043007 (2016).